Active Sites Speciation of Supported CoMoS Phase Probed by NO Molecule: A combined IR and DFT Study

Fabien Caron, Mickael Rivallan, Severine Humbert, Antoine Daudin, Pascal Raybaud, Silvia Bordiga

Active Sites Speciation of Supported CoMoS Phase Probed by NO Molecule: A combined IR and DFT Study

Fabien Caron,[a] *Mickaël Rivallan,*[a] *Séverine Humbert,*[a] *Antoine Daudin,*[a] *Silvia Bordiga,*[b] *Pascal Raybaud*[a,*]

[a] IFP Energies Nouvelles, Rond-point de l'échangeur de Solaize, BP 3 69360 Solaize (France)

[b] Dipartimento di Chimica NIS Centre and INSTM - Centro di Riferimento, Università di Torino, Via Quarello 15 Torino, I-10135 (Italy)

*corresponding author: Pascal Raybaud, IFP Energies nouvelles, email: pascal.raybaud@ifpen.fr

ABSTRACT

By using infrared spectroscopy and second derivative analysis, we identify key vibrational components of NO adsorbed the sulfided phases present in hydrodesulfurization (HDS) supported catalysts: MoS_2, cobalt promoted MoS_2 (CoMoS) and Co_9S_8. With the help of density functional theory (DFT) calculations, five components (A, A', B, B', C) identified by the second derivative analysis are assigned to mononitrosyls and dinitrosyls species on the various Mo and Co sites of the MoS_2, CoMoS and on Co_9S_8 phases. In particular, the component (A') at ~1846 cm^{-1} is due to mononitrosyl species on Co sites of the partially promoted M-edge or to dinitrosyl species on Co sites of the fully promoted S-edge of the CoMoS phase. This component (A') appears as a descriptor of the promoted sites and is present on the δθ- and γ-Al_2O_3 supports. By contrast, on silica supported catalyst, (A') decreases significantly in favor of component (A) at 1859-1863 cm^{-1} assigned mainly to nitrosyls on Co_9S_8 sites. Simultaneously, on silica, the component (B) at 1788-1790 cm^{-1} is assigned to dinitrosyls on the non-promoted Mo-edge and/or Co promoted S-edge and can be distinguished from the component (B') at 1799 cm^{-1} assigned to nitrosyls on the Co_9S_8 phase. A complementary chemometric analysis highlights that different evolution of the sites population as a function of NO contact time occurs as a function of the various sulfided phases and supports. In particular, chemometry suggests the presence of the two edges on the non-promoted MoS_2 phase. We finally discuss the implication of these findings for HDS catalysts.

KEYWORDS: MoS_2, CoMoS, alumina, silica, NO, infrared, density functional theory, hydrodesulfurization

1. INTRODUCTION

Due to the evolution of the worldwide environmental concerns, hydrodesulfurization (HDS) is a key industrial catalytic process to reach the targeted specifications on cleaner diesel and gasoline by removing undesirable sulfur compounds in petroleum feeds.[1] The industrial catalysts are usually based on an active transition metal sulfides MoS_2 phase promoted by cobalt or nickel atoms.[1, 2]

The atomic scale understanding of HDS catalysts remains a major concern for current research in order to provide innovative pathways for improving their intrinsic performances by design leading to more efficient process. Regarding the active phase, several studies based on numerous characterization techniques such as XPS,[3] EXAFS[4, 5] and high resolution TEM[6, 7] were conducted to better understand the atomic scale features of the active phase. The MoS_2 phase is highly dispersed on the alumina support and reveals crystallites of 3-4 nm size, which are decorated at the edges by cobalt atoms in order to form a so-called mixed CoMoS phase.[8] Density functional theory (DFT) calculations have also brought relevant insights into the atomistic description of the active phase such as the morphology of the MoS_2 nano-crystallite,[9, 10] location of the promoters,[11] and its impact on electronic properties[12] and reactivity.[13] These studies have in particular highlighted the crucial role of the sites located at the edges or close to the edges of the MoS_2 nano-crystallites.[14]

Further investigations of the active sites of HDS catalysts have used probe molecule adsorption followed by Fourier transform infrared spectroscopy (FTIR).[15] For instance, pyridine has been used to probe the Lewis and Brønsted acid sites of the MoS_2 and Co(Ni)MoS phase, leading to its protonation in presence of sulfhydryl groups at the edges.[16, 17] CO molecule has also been widely used to differentiate the coordinatively unsaturated sites (CUS) Mo and Co sites located at the edge of the MoS_2 nano-crystallites according to their local structure and coordination, although some open questions remain on the precise nature of these sites.[18, 19]

Nitric oxide (NO) probe is widely used in the literature to depict the surface atoms speciation present on $DeNO_x$ catalysts.[20-23] Moreover, NO has also been used to shed light into the surface state of the CoMoS active phase catalyst and into the nature of active edge sites.[24-28] Contrary to CO, it has been shown that NO is able to probe all the active sites of the CoMoS without being affected by the sulfur coverage. In particular, Tøpsøe et al. [27] have shown that NO molecules adsorption on the sulfided phase could lead to a total removal of the S atoms at 298 K via a so-called "push-pull" mechanism. In the same study, a first assignment has been proposed for main vibrational contributions of NO bond considering the non-promoted edges and promoted S-edge, but excluding the promotion of the M-edge,[27] which seems not fully consistent with previous DFT calculations[10, 11] and CO FTIR experiments.[29]

Moreover, this atomic scale understanding cannot be decoupled from considering the direct or indirect role played by the support which is a key component of the catalyst. Industrially, γ-alumina is the most widely used support in HDS of middle distillates into gasoil products[1, 30] but for specific applications such as HDS of gasoline produced by fluid catalytic cracking gasoline, other alumina polymorphs such as δ-alumina[7] may be preferentially chosen. At the laboratory scale, changing the nature of support (such as silica, zirconia, titania) has also revealed significant effect on the catalytic activity[31-36] and selectivity.[36-38] The support is thus suspected to impact the nature and intrinsic properties of the active sites linked to the number of promoter atoms engaged in the MoS_2 phase [34] or even the nano-structure (size, morphology) [35, 39] of the catalytically active phase.

In the present work, we propose to go beyond those previous studies related to the NO-FTIR, in order to investigate in more details the edge sites of the MoS_2 and CoMoS nano-crystallites and to highlight the speciation sensitivity on the type of support. For that purpose, we will first characterize $CoMoS/\delta\theta\text{-}Al_2O_3$ catalysts as well as $MoS_2/\delta\theta\text{-}Al_2O_3$ and $Co_9S_8/\delta\theta\text{-}Al_2O_3$ reference materials (Section 3.1). Then, with the help of DFT calculations extended to two types of possible edges, we will provide a detailed assignment of the IR-spectrum analysed through its second derivative (Section 3.2). In section 3.3, we will analyze

the effect of three relevant supports ($\delta\theta$-Al_2O_3, γ-Al_2O_3, and SiO_2) on the spectral features of the CoMoS edges. We underline that it is be beyond the scope of the present work to identify the origin of the this support effect. By changing the support, we aim at changing the nature of the active phase and explore the evolution of its spectral features. Section 3.4 will be devoted to chemometric treatments on IR spectra series which provide additional insights on the evolution of site population as a function of NO contact time. Finally, in section 3.5 we will discuss some implications for catalysis.

2. METHODS

2.1.Catalysts preparation

The different transition metal sulfides were prepared by incipient wetness impregnation on three different supports: γ-Al_2O_3, $\delta\theta$-Al_2O_3 and SiO_2. Silica support was provided by Norpro St Gobain as porous pellets (crushed and sieved in a diameter range of 0.315-1 mm). The alumina supports were provided by IFPEN as trilobal extrudates (length of around 2-4 mm with diameter of 1.6 mm). γ-Al_2O_3 was obtained by kneading-extrusion of boehmite powder followed by calcination at 813 K. and $\delta\theta$-Al_2O_3 by high temperature calcination (1223 K) from γ-Al_2O_3 extrudates. XRD of both aluminas and textural properties of the supports are reported in **supporting information 1**.

Impregnation solutions were prepared from MoO_3 and $Co(OH)_2$ precursors dissolved in aqueous solution in presence of H_3PO_4. Impregnation was performed on the three supports followed by an ageing step for 12 h to allow metal diffusion throughout the extrudates or pellets. Then, solids were dried in an oven at 393 K for 24 h and calcined in air at 723K for 2h15. Finally, oxide catalysts are presulfided *ex situ* by heating at 5 $K.min^{-1}$ from 298 to 623 K at atmospheric pressure in a flow of 15 vol.% H_2S in H_2 (1.5 $L.h^{-1}g^{-1}$ of catalyst). Sulfidation was achieved at 623 K for 2h15min. *Ex situ* sulfided materials were then isolated under vacuum at 473 K in a sealed glass flask.

105 On each support, molybdenum loadings were selected to obtain fixed molybdenum surface densities
106 (labeled dMo in what follows) of 2.2 atoms by nm² of support. In order to compare catalysts at iso-dMo
107 and iso-support, Co/Mo and P/Mo molar ratios are also kept constant at 0.4 and 0.27 respectively.
108 $MoS_2/\delta\theta\text{-}Al_2O_3$ and $Co_9S_8/\delta\theta\text{-}Al_2O_3$ reference materials are also prepared on $\delta\theta\text{-}Al_2O_3$ (according to the
109 same preparation procedure mentioned above for CoMoS supported catalysts). The XRF elemental
110 analysis of Co, Mo and P on different supports (**supporting information 1**), ensures the consistency with
111 the targeted elemental contents.

112 2.2 FTIR experiment

113 Characterization NO-FTIR experiments were performed with a static experimental set-up under vacuum.
114 An IR cell made in quartz equipped with KBr windows was used. The *ex situ* sulfided catalyst powders
115 were pressed and used as wafer of 16 mm diameter and ca. 20 mg which represent 10 $mg.cm^{-2}$ under
116 controlled atmosphere (argon). Catalyst wafer was introduced in the IR cell under argon. Prior to NO
117 contact, the cell was evacuated under primary vacuum and closed. The vacuum line is then filled with NO
118 at pressure equilibrium of 150 mbar. NO was afterwards expanded in the FTIR cell to reach 70 mbar
119 equilibrium pressure. Interactions of NO on the surface of the sulfided catalyst wafer are followed by
120 FTIR as function of time. After 5 min NO contact, the gas phase spectra were recorded and the in situ
121 FTIR cell and Schlenck line were evacuated under primary vacuum. A spectrum of the catalyst after NO
122 evacuation was also recorded. Subtractions of IR spectra of the catalyst wafer under vacuum before
123 adding NO (reference spectrum) and of the NO gas phase spectra to catalyst wafer under NO atmosphere
124 were performed in order to evidence the IR contributions of the stable nitrosyl species sorbed on the
125 surface of sulfided phases: CoMoS, MoS_2 and Co_9S_8. Second derivatives of the IR spectra absorbance of
126 the NO sorbed on $\delta\theta\text{-}Al_2O_3$ supported catalysts were calculated with a Savitzky-Golay function (9 points,
127 3 order polynomial).

2.3 Chemometric method

Chemometric calculations were performed by using the multivariate curve resolution-alternating least squares (MCR-ALS) method directly on the subtracted FTIR spectra. MCR-ALS is based on a linear model assuming the generalized law of Lambert–Beer where the individual response of each component is addable. The aim of this mathematical method[40] is the decomposition of the original data matrix D, which contains all the spectra recorded during NO contact (from t = 0 to 5 min), into the product of two matrices, C and S^T, $D = C.S^T + E$ where C and S^T contain the calculated concentration profiles and corresponding reference IR signals respectively. The error of the fit is contained in matrix *E*. We apply a single constraint of non-negativity for the concentration profiles and reference spectra. This method has already been successfully applied for size discrimination of supported Pt particles,[41] however to the best of our knowledge, it has not been yet applied to FTIR spectra of supported sulfides catalysts.

2.4 DFT calculations

2.4.1 Total energy

Periodic density functional calculations have been performed using the VASP code.[42-44] Spin polarized general gradient approximation (GGA) with the PW91[45, 46] exchange correlation functional and projected augmented-wave (PAW) formalism have been used for total energy calculations. The cut-off energy for the plane-wave basis was fixed to 500 eV and the Brillouin zone integration is performed on a (3×3×1) k-point mesh for the supercell described in the next section with a Methfessel and Paxton smearing method (σ=0.1).

2.4.2 Models

Relevant examples of the periodic supercells and technical aspects related to them are described in details in the **supporting information 2**. Previous DFT studies [9-11] have shown the impact of the chemical

potential of sulfur on the sulfur coverages and 2D morphology of non-promoted and Co promoted MoS_2 crystallites. In sulfo-reductive conditions such as the one used in the experimental section for activating the sulfided phase (623 K and $pH_2S/pH_2 = 0.18$), the predicted shape for non-promoted MoS_2 crystallites is a deformed hexagon where 70-75% of the edges are made of the so-called M-edge and 30-25% of S-edge. For the Co-promoted MoS_2, the shape is close to an hexagon. DFT calculations were performed in order to determine the most stable adsorption mode of NO on these M- and S-edges of the MoS_2 and CoMoS phases for various S and NO coverages. Nevertheless, it was shown by Topsøe et al. that the adsorption energy of NO is so high that the NO molecule could displace/remove the S-atoms via a "push-pull" mechanism (trend confirmed by the present study, see further). Thus, the equilibrium S-coverage found in H_2S/H_2 environment becomes unstable in presence of NO and we consider in what follows, configurations where S-atoms have been fully removed at the edge and replaced by NO molecules. **Table S2.1** reports the various S-coverages at S- and M-edges and their local configurations considered for probing NO adsorption.

2.4.3 Geometry optimization and adsorption energy

The geometry optimization has been completed when the convergence criteria on forces becomes smaller than 0.02 eV/Å. The configurations reported here, result from geometry optimization performed in two steps: (i) First the bare surface composed of four (or five in the case of CoMoS) atomic layers have been fully optimized, (ii) Then the geometry of the adsorption of the *n*NO molecules adsorbed on the adsorption sites has been optimized, relaxing the atoms of the molecules and the ones of the two atomic layers of the surface, and fixing the position of the atoms of the two (or three) deepest atomic layers. Once the most stable configuration is found, the adsorption energy of the NO molecules (ΔE_{ads}) is calculated at 0 K using the following expression:

$$n\Delta E_{ads} = E(n\mathrm{NO} - \mathrm{stripe}) - E(\mathrm{stripe}) - nE(\mathrm{NO}) \quad (1)$$

174 E(stripe) is the energy of the stripe representing the reference bare MoS_2 or CoMoS edge, E(nNO –
175 stripe) is the energy of the nNO molecules adsorbed on the corresponding edge and E(NO) is the energy
176 of the isolated NO molecule.

177 For some specific configurations where the stability of the reference bare MoS_2 or CoMoS edge is not
178 stable, we calculate the exchange energy corresponding to the removal of n sulfur atoms upon the
179 adsorption of nNO molecules:

$$\Delta E_{exch} = E\big(n\mathrm{NO} - (\mathrm{stripe} - n\mathrm{S})\big) - E(\mathrm{stripe}) - n(E(\mathrm{NO}) - E(\mathrm{H_2S}) + E(\mathrm{H_2}))$$

180 $E\big(n\mathrm{NO} - (\mathrm{stripe} - n\mathrm{S})\big)$ is the energy of the nNO molecules adsorbed on the edge where nS atoms have
181 been removed, $E(H_2S)$ and $E(H_2)$ are the energies of the isolated H_2S and H_2 molecules.

182 2.4.4 Frequency calculations

183 Harmonic frequency calculations for the NO molecules were performed with VASP through numerical
184 differentiation of the force matrix, including all vibrational degrees of the atoms of the molecules and of
185 the metallic atoms of the adsorption site. Including the relaxation of the neighboring sulfur atoms of the
186 adsorption sites does not impact the frequency values reported here. The calculations were performed on
187 the configuration that was previously subjected to a geometry optimization. The displacement step was
188 fixed to 0.02 Å. In order to compare the theoretical frequencies to the experimental frequencies, a scaling
189 factor of 0.985 is used, which corresponds to the ratio between the experimental frequency of the NO
190 molecule in gas phase (1876 cm^{-1}) and the calculated frequency of the isolated NO (1905 cm^{-1}).

191

192

193

194 3. RESULTS AND DISCUSSION

195 3.1 Case of δθ-Al_2O_3 supported samples

196 3.1.1 IR analysis

197 IR spectra of NO adsorbed on the calcined Mo, Co and CoMo oxides and the CoMoS sulfide (obtained by

198 sulfo-reduction of the CoMo oxide) supported on δθ-Al_2O_3 are shown in **Figure 1**.

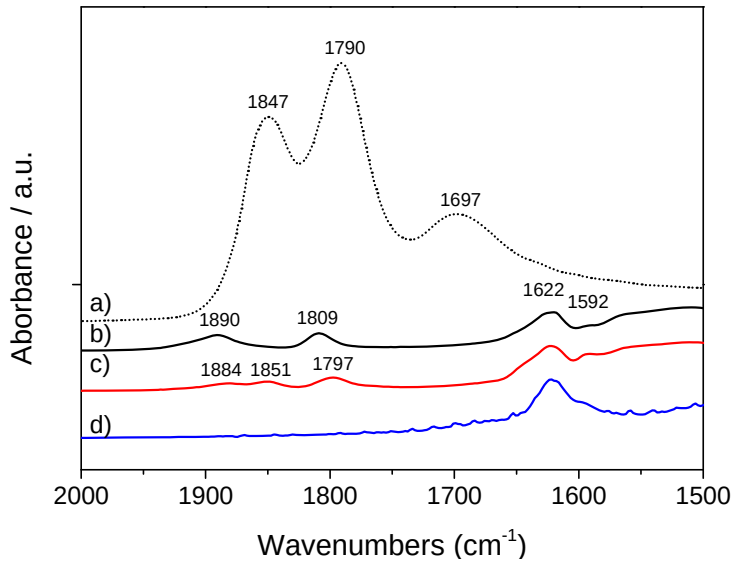

199

200 **Figure 1.** IR spectra (background subtracted and normalized by the mass of the wafer) of NO adsorbed

201 on δθ-Al_2O_3 supported Mo (d) in blue, Co (c) in red, CoMo oxides (b) in black. For comparison, sulfided

202 CoMoS (a) in dotted line) after 5 min contact in NO (P = 70 mbar) and subsequent evacuation at 298K is

203 reported.

204

205 In the spectra obtained for metal oxides supported on δθ-Al_2O_3, two regions can be distinguished: at 1650

206 – 1500 and at 2000 – 1650 cm^{-1} which are attributed to nitrite/nitrate species formed upon NO contact and

207 to nitrosyl adsorbed on the surface of the oxide or sulfided phases respectively. The contributions of NO

208 adsorbed on the oxides Mo, Co and CoMo supported on δθ-Al_2O_3 are weak. Indeed, for calcined Mo/ and

209 Co/δθ-Al_2O_3 samples, Mo and Co are present as Mo^{6+} and Co^{2+} (d^0 and d^5 states respectively) which are

not expected to adsorb strongly NO molecule.[28] For cobalt oxide supported on δθ-Al_2O_3 (spectrum c, Figure 1) three distinct NO contributions appear at 1884, 1851 and 1797 cm^{-1} in the nitrosyl region. The two bands at 1884 and 1797 cm^{-1} are due to the formation of $Co^{2+}(NO)_2$ complexes (ν_s(NO) and ν_{as}(NO) modes respectively), while the band at 1851 cm^{-1} is assigned to mononitrosyl Co^{2+} species.[20] The oxide Mo/δθ-Al_2O_3 material (spectrum d, Figure 1) does not display any contribution due to nitrosyl species in the spectrum. In that case, only nitrite/nitrate species formation is observed (1620 and 1592 cm^{-1}).[47] Considering the CoMo oxide material (spectrum b), two contributions are found at 1890 cm^{-1} and 1809 cm^{-1}. These components are close to those observed for the oxide Co/δθ-Al_2O_3 sample and could be assigned to similar $Co^{2+}(NO)_2$ species.[20] It is interesting to note first that the dinitrosyl contributions are more intense than on Co/δθ-Al_2O_3 and secondly that mononitrosyl species is not observed on CoMo sample. It may indicate that cobalt oxide is better dispersed when introduced in presence of molybdenum. The nature of the species in the aqueous solution of impregnation should be different and may lead to different state of metal dispersion.

For comparison, NO titration have been undertaken on sulfided CoMoS materials and the corresponding IR spectrum after NO saturation reports three distinct contributions in the 1850 – 1700 cm^{-1} range (**Figure 1**). The contributions are much more intense compared to the oxide materials due to i) the great affinity of NO for edge sites of the promoted or non-promoted sulfided phases and the surface sites of Co_9S_8, ii) the possible higher molar absorption coefficient of nitrosyls adsorbed on the sulfided phase and iii) the higher concentration of surface sites prompt to adsorb NO. Thus, NO is a relevant probe molecule of the sulfided phase in agreement to previous works.[20] Under specific conditions, NO molecule was claimed to be a reactive probe towards the sulfided phase which might be oxidized.[48] In the present case, one can nevertheless remark that unlike supported metal oxide, oxidation mechanisms with further formation of nitrite or nitrate species remain very limited on CoMoS catalyst in interaction with NO at 298 K in agreement with data reported in former works.[20, 24-28]

234 The IR spectra of NO adsorbed on sulfided CoMoS and references MoS_2, Co_9S_8 supported on δθ-Al_2O_3

235 with constant Mo loading and Co/Mo ratio are shown in **Figure 2a**.

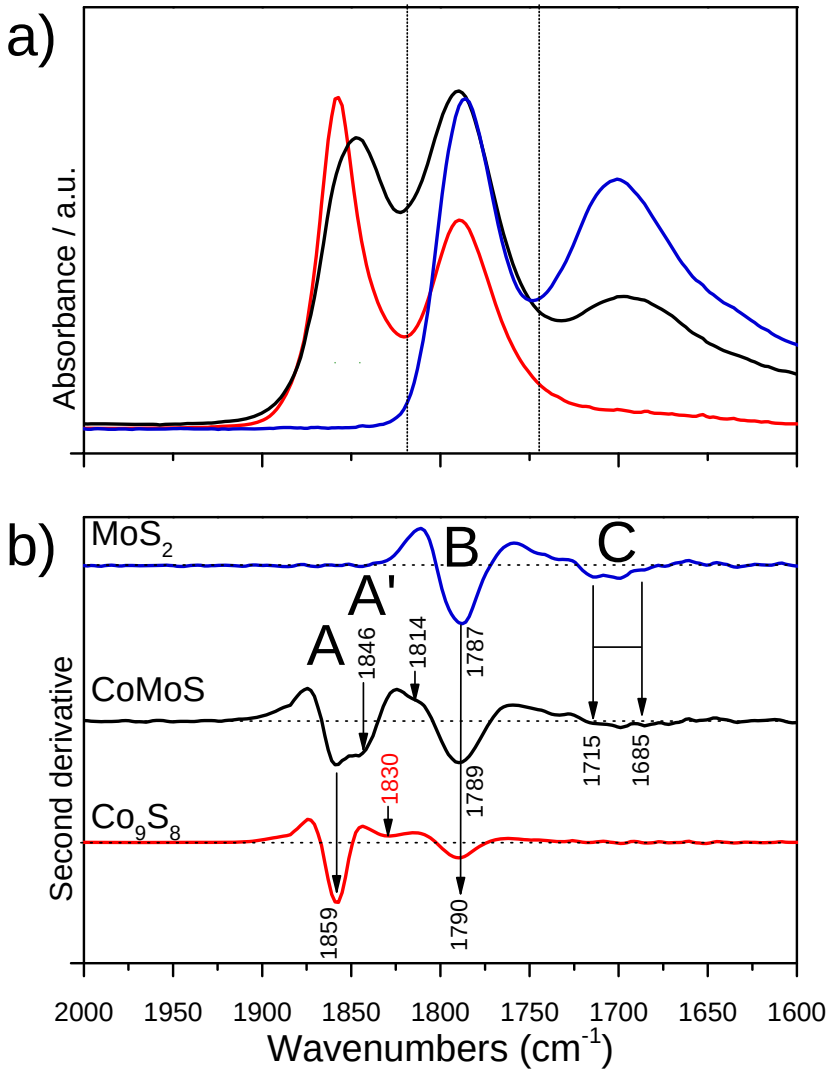

236

237 **Figure 2**. a) IR spectra of the sulfided catalysts: MoS_2 (blue), Co_9S_8 (red) and CoMoS (black) supported

238 on δθ-Al_2O_3 (normalized by gram of catalyst) after 5 min contact in NO (P = 70 mbar) and subsequent

239 evacuation at 298K; b) Second derivative of the IR spectra (similar code color) with minima identified

240 according to the method described in **supporting information 3**.

241

As previously discussed, three components are observed in the IR spectra recorded at NO saturation for the series of samples supported on δθ-Al_2O_3 : 1880 – 1840 cm^{-1} ; 1810 - 1790 cm^{-1} and 1715 - 1685 cm^{-1} (broad) which will be hereafter referenced as (A), (B) and (C) components respectively. The IR spectrum of NO on the Co sulfided material gives rise to (A) and (B) components while, IR spectrum of Mo sulfided sample in interaction with NO exhibits two contributions (B) and (C). From the comparison with NO adsorption complexes and metal cluster complexes, these two absorption bands have been tentatively assigned to the symmetric and asymmetric stretching vibrations of dinitrosyl species adsorbed on the edge sites of the CoMoS and MoS_2 phases.[24] It can be noticed that (B) and (C) components are also close to those generally observed for reduced Mo supported catalyst in interaction with NO.[47, 49, 50] However, IR NO spectra obtained on CoMoS /δθ-Al_2O_3 reveals (A), (B) and (C) components which seem to result from the superposition of the two doublet bands observed for MoS_2/δθ-Al_2O_3 and Co_9S_8/δθ-Al_2O_3.[24, 51-53] Hence, vibrational contributions of NO adsorbed on MoS_2 and Co_9S_8/δθ-Al_2O_3 overlap and are very close with the contributions of NO adsorbed on CoMoS on δθ-Al_2O_3. This makes thus difficult to identify the contributions due to the nitrosyl species adsorbed on the edges of the promoted CoMoS slabs without further treatments of the IR spectra as proposed in what follows.

3.1.2 Analysis of the second derivative of the IR spectra

To obtain a more detailed description of the vibrational contributions observed after NO contact on CoMoS, MoS_2 Co_9S_8, the second derivative of the IR spectra was plotted in **Figure 2 b** and the minima have been identified according to the analysis reported in **supplementary information 3** considering the evolution as a function of the contact time. **Table 1** reports the corresponding vibrational frequencies obtained from this analysis. As revealed in **Figure 2b**, second derivative analysis obviously allows the identification of minor contributions (**supplementary information 3**) and also overlapping ones which are not resolved in the initial spectrum. This analysis was proposed recently on non-promoted MoS_2

phase.[25] The second derivative spectra obtained for NO adsorbed on δθ-Al_2O_3 supported Co_9S_8 and MoS_2 confirm the existence of two doublets already visible in the initial spectra: (A) 1859 / (B) 1789 cm^{-1} and (B) 1787 cm^{-1} / (C) 1715 – 1685 cm^{-1} respectively. It should be noted that the region corresponding to the (C) component contains actually several contributions with lower intensities than in (A) and (B) component (**supplementary information 3)**. The CoMoS/δθ-Al_2O_3 catalyst reveals three intense contributions : (A) 1859 cm^{-1}, (A') 1846 cm^{-1}, (B) 1790 cm^{-1} and more broaden contributions within the (C) component region. The three contributions (A), (B) and (C) reveal that either CoMoS phase exhibits edge sites with similar electronic properties as the non-promoted Mo edge and Co_9S_8 sites or that non promoted MoS_2 crystallites and/or Co_9S_8 phases are present. However, the component located at 1846 cm^{-1} (A') appears as a specific feature of the promoted CoMoS phase. Hence, the two contributions (A) and (A') overlapping in the IR spectrum of CoMoS/δθ-Al_2O_3 are now distinguished: (A) being assigned to Co_9S_8 sites and (A') to CoMoS. Moreover, it appears that the intensity of the bands at 1715 – 1685 cm^{-1} corresponding to the (C) region is less pronounced for the CoMoS catalyst than for the non-promoted one.

Table 1. Observed components of the NO adsorbed on the sulfided MoS_2, Co_9S_8 and CoMoS phases supported on δθ-Al_2O_3.

Region	ν (cm^{-1})	CoMoS	MoS_2	Co_9S_8
A	1859	✓		✓
A'	1846	✓		
B	1790 – 1787	✓	✓	✓
C	1715 – 1685	✓	✓	

It must be added that minor components are also identified at different wavenumbers for the different samples (**supporting information 3**). Some of these vibrational contributions are present exclusively on the CoMoS sample such as 1814 cm^{-1}, while the minor contribution at 1830 cm^{-1} seems to be specific of

the Co_9S_8 phase. These major or minor components will be considered for the forthcoming comparison with DFT calculations. These features are probably key to identify the CoMoS phase and will be further discussed with DFT calculations and its evolution will also be considered with respect to other supports.

3.2 DFT calculations of NO adsorption on MoS_2 and CoMoS edges

Before providing a direct comparison with experimental results, it is worth presenting a preliminary theoretical analysis of NO adsorption on the different type of sites at low NO coverage in order to provide some general chemical trends.

3.2.1 M-edge at low NO coverage

As expected the adsorption energies are significantly higher (ΔE_{ads} from -177 to -362 kJ/mol, **Table S2.2**) than those calculated for the CO molecule on similar systems (smaller than -140 kJ/mol).[18, 19] Due to the presence of the unpaired electron in the $\pi*$ orbital of NO, this molecule is highly reactive and interacts more strongly with any Lewis Mo or Co sites than CO. The adsorption energy on Mo site is about -362 kJ/mol for the non-promoted site, which is significantly higher than for the adsorption energy of one sulfur atom on the same site (~ -250 to -295 kJ/mol).[54] On the Co site, this trend is even more pronounced: ΔE_{ads}=-242 kJ/mol whereas the adsorption energy of one sulfur atom is about ~20kJ/mol.[55] Thus, this analysis confirms that NO molecule certainly replaces or displaces S atoms at the edge as proposed in a previous work.[27]

Moreover, **Table S2.2** shows that the adsorption energy of NO molecule is more favorable on any Mo Lewis acid sites (when no sulfur atom is present), while the downward frequency shift is significantly larger on Mo than on Co sites: the difference between the two sites is close to 200 cm^{-1} for the ideal case of isolated mononitrosyl species. This trend results from two intricate effects: on the one hand, the acceptor character (involved in the donation) of the Co site is weaker than the one of the Mo site, on the

other hand, the δ-π overlap (resulting from back donation) is also weaker for the Co-3*d* electrons than for the Mo-4*d* electrons. Although these preliminary configurations on edge sites at low coverages are not obligatory relevant for our IR experiments, they readily help to understand the intrinsic site-driven parameters of the vibrational frequencies of NO adsorbed on the CoMoS systems. The experimental main bands are covering a wide frequency range of about 170 cm^{-1} where Mo sites should generate vibrational frequencies located at the lower region of the IR spectrum (C band), whereas Co sites on the M-edge may impact the upper region (close to the A band).

In addition, the vibrational frequency depends on the nature of the neighboring sites and local environment on the edge. In particular, on the partially promoted M-edge, the presence of Co atoms in the close vicinity of the Mo site where NO is adsorbed, induces a slight increase of the vibrational frequency (+20 to 25 cm^{-1}). Conversely, the presence of Mo atoms in the close vicinity of the Co site where NO is adsorbed induces a slight decrease of the vibrational frequency (-34 to -37 cm^{-1}).

Another environment effect may be studied here by considering the presence of sulfur atoms on the neighboring sites. For the non-promoted and promoted M-edge, adding 2 or 3 sulfur atoms on the neighboring sites where NO is adsorbed leads to an increase of the vibrational frequency by up to + 40 – 50 cm^{-1}. This may be considered as a surface coverage effect with dipole-dipole interaction between the neighboring Mo-S and Mo-NO species due to the overlap between the Mo 4*d* electrons and π∗ orbital of NO.

3.2.2 S-edge at low NO coverage

If we now consider the adsorption of NO on the S-edge, **Table S2.3** shows that on the non-promoted S-edge with a S-coverage of 50% as encountered in usual sulfidation conditions, the NO adsorption energy is significantly lower than on the M-edge with 0% S (Mo sites are 4 fold coordinated in both cases). At the same time, the corresponding vibrational frequency is also higher at 1726 cm^{-1} for the isolated

mononitrosyl. If we consider the higher S-coverage (100%), the calculated NO vibrational frequency is even higher 1760 cm^{-1}. As a consequence, in these two S-edge cases as well as for the M-edge, it appears difficult to find Mo sites where the NO vibrational frequency is greater than 1800 cm^{-1}, which seems to be consistent with the experimental observations where the two main observed bands (B and C) are below 1800 cm^{-1}.

By contrast, considering the Co-promoted S-edge with S-coverage of 75%, when NO is adsorbed on top of a Co site, it is observed that the calculated adsorption energy is significantly lower than on the M-edge while the vibrational frequency is equal to 1864 cm^{-1} as high as for the Co site on the M-edge with neighboring S-sites. This may indicate again that NO adsorbed on Co sites are generating bands in the high frequency region (A), however due to the rather low adsorption energy on this Co S-edge site, this low coverage configuration may not be considered as relevant.

It should also be noticed that when one S atom is exchanged by one NO molecule in a bridging position, the NO vibrational frequency decreases tremendously at 1456 cm^{-1}. A similar trend is observed for the Co-promoted S-edge (1574 cm^{-1}, **Table S2.3**) and for the non-promoted M-edge (for specific NO bridging position not reported here). These low frequency values do not match any of the main observed IR bands. Considering the analysis of the second derivatives of the absorbance, one may not exclude that some minor contributions at low frequencies could be eventually assigned to isolated defect sites, if not beyond the experimental accuracy.

3.2.3 Effect of NO coverage

Due to the rather strong adsorption energy of NO adsorbed on the Mo or Co sites (often more than -200 kJ/mol), it is expected that even small doses of NO as used experimentally may lead to high NO coverage at the edges, even if the S-coverage after sulfo-reducing conditions would be high. Hence, the S-exchange process will be thermodynamically favored, and may lead to the complete removal of S-atoms on the

edges and allowing several NO molecules to be adsorbed.[27] Thus, the sulfur coverage should drastically diminish with respect to the sulfiding conditions, while the NO coverage increases as a function of the experimental pressure of NO applied.

- *Case of the non-promoted edges*

Considering first the non-promoted M-edge, increasing the NO coverage may lead either to dinitrosyl species or neighboring mononitrosyls which exhibit coupled vibrational modes: generally one symmetric and one asymmetric mode. If these species are assumed to be isolated, **Table 2** shows that the adsorption energies remain highly exothermic in both cases, while the symmetric modes exhibit higher frequencies (1705 and 1718 cm^{-1} respectively) than the isolated mononitrosyl (1671 cm^{-1}). This trend is also consistent with previous DFT calculations on $Mo_{16}S_{32\pm x}$ clusters.[56] This well-known coverage effect results from the through space interaction of the Mo-NO dipole leading to dynamic shifts of about +34 to +47 cm^{-1} which are in line with those reported for NO on NiO surface.[57] At the same time, the asymmetric modes appear at significantly lower frequencies (1604 and 1670 cm^{-1} respectively.)

If the NO coverage is increased up to one dinitrosyl species per Mo site (saturation level in the experiments), an even broader distribution of frequencies is found from 1625 cm^{-1} to 1809 cm^{-1}. Moreover, it appears that the adsorption energy for the multiple mononitrosyls remains high ~ -343 kJ/mol which means that the energy required to exchange the 4 S bridging atoms obtained at equilibrium in H_2S/H_2 environment is estimated at about ΔE_{exch} =-160 kJ/mol.[54] A similar exothermic exchange energy is found for the multiple dinitrosyl configuration. Thus, this confirms that thermodynamically these S-atoms can be removed from the edge by NO at high coverage.

A fruitful assignment is furnished in **Table 2:** it can be noticed that the increase of NO coverage induces the appearance of higher frequencies closer to the IR region (B) located around 1787 cm^{-1} on the experimental spectrum of the non-promoted MoS_2. This component (B) can be due to the symmetric coupling of mononitrosyls or dinitrosyls as shown by DFT calculations (**Table 2**). Several lower

frequencies at 1714, 1700 and 1685 cm^{-1} (**supporting information 3**) of component (C) correspond to asymmetric coupling of mononitrosyls (calculated at 1708 cm^{-1}) or of dinitrosyls (1712 and 1688 cm^{-1}).

Table 2. Calculated adsorption energies and corresponding vibrational frequencies of NO adsorbed on the various possible M- and S-edge sites of non-promoted MoS_2 at various NO coverages. Green balls: molybdenum, yellow balls: sulfur, blue balls: cobalt, dark blue balls: nitrogen, red balls: oxygen.

Site	Configuration		ΔE_{ads} (kJ/mol NO)	Calculated ν_{NO} (cm^{-1})[a]	Experimental ν_{NO} (cm^{-1})[b]
Mo on the non-promoted M-edge 0%S	Dinitrosyl	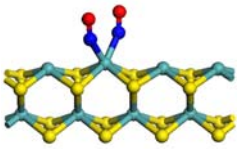	-224	1705_s[c] 1604_a	**1787 (B)** 1747, 1733 **1714 (C)** **1700/1685 (C)** 1672 1650 1637
	Coupled mononitrosyl	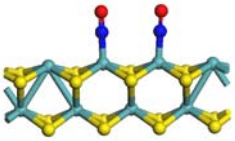	-349	1718_s 1670_a	
	Multiple mononitrosyl	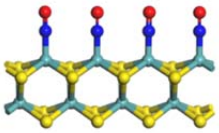	-343	**1769_s (B)** **1708_a (C)** **1708_a (C)** 1660_a	
	Multiple dinitrosyl	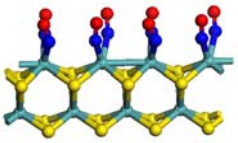	-189	**1809_{ss} (B)** 1762_{sa}, 1740_{sa} **1712_{sa} (C)** **1688_{as} (C)** 1659_{aa}, 1650_{as} 1625_{as}	
Mo on the non-promoted S-edge 50%S and 0%S	Multiple Mononitrosyl	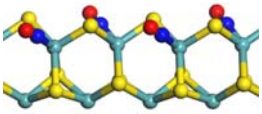	-167	1763 1745 1738 1736	
	Multiple dinitrosyl	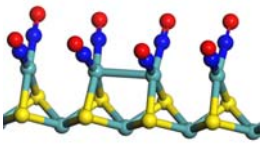	-136[d]	**1831_{ss} (B)** 1772_{sa}, 1770_{sa}, 1768_{as} 1739_{sa}, 1731_{aa}, 1727_{aa} **1693_{aa} (C)**	

[a] vibrational frequency is corrected by a factor of 0.985 (see methods for explanation).
[a] and [b] bold values correspond to the experimentally observed main regions (A), (B) or (C). Non bold values correspond the minor contributions also identified in the second derivative analysis (**supporting information 3**).
[c] abbreviation for modes: s=symmetric mode, a=antisymmetric, ss=symmetric within each dinitrosyl complex and between all neighboring sites, sa= symmetric within each dinitrosyl complex and antisymmetric between neighboring sites, as=antisymmetric within each dinitrosyl complex and symmetric between neighboring site, aa= antisymmetric within each dinitrosyl complex and antisymmetric between neighboring site.
[d] exchange energy ΔE_{exch}

Finally, as reported in **Table 2**, other minor contributions at lower frequencies such as 1672 and 1650 and 1637 cm^{-1} (**supporting information 3**) are also recovered by the DFT calculations and they should correspond to both mononitrosyls and dinitrosyl species. These experimental values as well as their DFT assignment are generally coherent with the previous experimental work[25] with the exception that the minor lower frequencies (1637 cm^{-1}) cannot be assigned to isolated mononitrosyls as proposed by van Haandel et al. but rather to asymmetric-symmetric coupling between dinitrosyls. Due to their very low intensities in the second derivative analysis, it may probably be difficult to assign them without ambiguity on the pure basis of experiments.

As recalled in the methods, previous DFT calculations[10, 11] have predicted that the shape of the MoS_2 crystallite is a deformed hexagon where 70-75% of the edges are constituted of the M-edge in sulfo-reductive conditions as used for the synthesis of the sulfided catalyst. Hence, we have checked the vibrational frequencies in the cases of the multiple mononitrosyls and dinotrosyls adsorbed on the S-edge with 50% S and 0% S respectively. Apparently the multiple dinitrosyls configuration leads to vibrational frequency calculated at 1831 cm^{-1} which seems a little bit too high to fully agree with experimental component (B). The calculated frequency at 1693 cm^{-1} falls within the range of component (C) but does not fully recover all contributions of component (C). Even if one cannot fully rule out the contribution of the S-edge, the predominance of the M-edge should be sufficient to interpret the experimental observations. This point will be further discussed with the chemometry analysis.

- *Case of the promoted edges*

On the cobalt promoted M-edge with 50% cobalt and 50% Mo sites, the dinitrosyl species cannot be stabilized on Co sites where only mononitrosyl species are stable. On the Mo site, **Table 3** shows that the two NO vibrational frequencies corresponding to the symmetric and asymmetric modes are shifted to

417 higher values (1772 and 1708 cm^{-1} respectively) than the ones of the non-promoted edge. This trend
418 confirms the non-negligible effect of the chemical nature of neighboring sites on the NO vibrational
419 frequencies. For the highest NO coverage which corresponds to the saturation level, Mo sites are thus
420 covered by dinitrosyls and Co sites by mononitrosyls which generate vibrational frequencies from 1639 to
421 1867 cm^{-1}. It should be stressed that the higher calculated frequencies reported in **Table 3** are induced by
422 the predominant contribution of NO adsorbed on the Co sites. This trend is in line with our previous
423 analysis on the low NO coverage regime, and highlights that the M-edge partially decorated by cobalt
424 may contribute to component (A') observed around 1846 cm^{-1} in the IR experiments to be specific of the
425 CoMoS/δθ-Al_2O_3 catalyst (**Figure 2b**). In addition, the frequency calculated at 1774 cm^{-1} may
426 correspond to component (B) observed on promoted MoS_2. By contrast, NO adsorbed on this edge (either
427 as multiple mononitrosyls or dinitrosyls) does not contribute strongly to the bands of component (C) at
428 1715 – 1685 cm^{-1}. By contrast, the minor contributions observed at 1734, 1672, 1657 and 1633 cm^{-1}
429 (**supporting information 3**) are recovered by the DFT calculations on this edge, which may indicate that
430 these bands are features of the CoMoS phase (even if some of them are also found on the MoS_2 phase.)

431 For NO saturating the cobalt sites located on the S-edge, two configurations are found very close in
432 energy. The first one (called parallel) exhibits dinitrosyl species present on each cobalt site lead to
433 vibrational frequencies in the range of 1650 to 1787 cm^{-1} with contributions in the range of components
434 (B) and (C) but not in component (A'). **Table 3** reveals a reasonable agreement between all calculated
435 frequencies and the experimental ones (major and minor components) analyzed by the second derivative
436 of the IR spectra. In this case, all NO molecules are lying in the same plane parallel to the edge surface
437 and each dinitrosyl species are aligned according to an ON---NO scheme.

438

Table 3. Calculated adsorption energies and corresponding vibrational frequencies of NO adsorbed on the various possible Co promoted M- and S-edge sites at various NO coverages. Same color legend as Table 2.

Site	Type	Adsorption configuration	ΔE_{ads} (kJ/mol NO)	Calculated ν_{NO} (cm^{-1})[a]	Experimental ν_{NO} (cm^{-1})[b]
Co on the promoted M-edge with 50% Co	Dinitrosyl	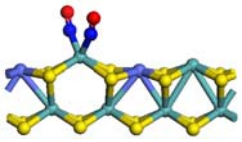	-206	1772_s[c] 1708_{as}	
	Coupled mononitrosyl	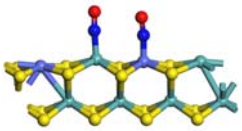	-251	$1858_{Co\text{-}s}$ $1655_{Mo\text{-}as}$	
	Multiple mononitrosyls	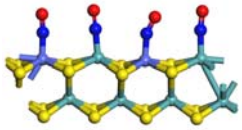	-251	$1887_{Co\text{-}s}$ $1808_{Co\text{-}s}$ $1662_{Mo\text{-}as}$ $1649_{Mo\text{-}as}$	**1846 (A')** 1814 **1790 (B)** 1734 **1716** (C) **1697/1685 (C)** 1672 1657 1634
	Multiple dinitrosyls	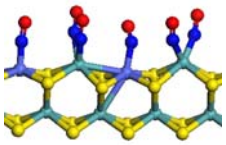	-184	**1867_{Co} (A')** **$1774_{Mo\text{-}ss}$ (B)** $1740_{Mo\text{-}sa}$, $1670_{Mo\text{-}aa}$ $1656_{Mo\text{-}as}$ $1639_{Mo\text{-}aa}$	
Co on the promoted S-edge with 100% Co	Multiple dinitrosyls parallel	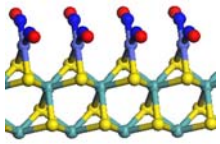	-108[d]	**1787_{ss} (B)** 1729_{sa}, **1720_{sa}/ 1719_{sa}/1689_{aa}/ 1686_{aa} (C)** 1678_{sa}, 1650_{aa}	
	Multiple dinitrosyls upright-tilted	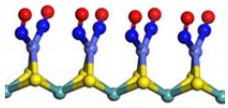	-106[d]	**1861_{ss} (A')** **1813_{sa}/1810_{sa}/ 1782_{sa} (B)** **1698_{as} (C)** 1657_{aa}, 1651_{aa}, 1614_{aa}	

[a] vibrational frequency is corrected by a factor of 0.985 (see methods for explanation).
[a] and [b] values written in bold correspond to the experimentally observed main regions (A), (B) or (C). Other values correspond to minor contributions also identified in the second derivative analysis (**supporting information 3**).
[c] abbreviation for modes: s=symmetric mode, a=antisymmetric, ss=symmetric within each dinitrosyl complex and between all neighboring sites, sa= symmetric within each dinitrosyl complex and antisymmetric between neighboring sites, as=antisymmetric within each dinitrosyl complex and symmetric between neighboring site, aa= antisymmetric within each dinitrosyl complex and antisymmetric between neighboring site.
[d] exchange energy ΔE_{exch}

Each Co atom sits in a perfect square planar environment formed by the dinitrosyl ligands and the two S-atoms. This interesting configuration would thus imply that the partially promoted M-edge and fully

promoted S-edge do not contribute exactly to the same IR bands: in particular, the S-edge would not contribute to the (A') component. This may provide an appealing way of distinguishing the two types of sites at high level of NO saturation.

For NO saturating the cobalt sites located on the S-edge, two configurations are found very close in energy. The first one (called parallel) exhibits dinitrosyl species present on each cobalt site lead to vibrational frequencies in the range of 1650 to 1787 cm^{-1} with contributions in the range of components (B) and (C) but not in component (A'). **Table 3** reveals a reasonable agreement between all calculated frequencies and the experimental ones (major and minor components) analyzed by the second derivative of the IR spectra. In this case, all NO molecules are lying in the same plane parallel to the edge surface and each dinitrosyl species are aligned according to an ON---NO scheme. Each Co atom sits in a perfect square planar environment formed by the dinitrosyl ligands and the two S-atoms. This interesting configuration would thus imply that the partially promoted M-edge and fully promoted S-edge do not contribute exactly to the same IR bands: in particular, the S-edge would not contribute to the (A') component. This may provide an appealing way of distinguishing the two types of sites at high level of NO saturation.

Nevertheless, a second configuration (called upright-tilted) must also be considered: it is only slightly less stable (2 kJ/NO) and one half of the NO molecules (belonging to distinct dinitrosyls) is oriented in a nearly upright position, and the second half is in a tilted position. This configuration was previously reported in a combined experimental and DFT work[27] and our calculated frequencies (**Table 3**) match well with these previous published ones. In this configuration, the symmetric coupling mode of the close to tilted NO molecules leads to a calculated frequency (1861 cm^{-1}) value that remain compatible with the (A') component. The antisymmetric coupling mode of the tilted NO molecules lead to a set of calculated frequencies (1813/1810/1782 cm^{-1}) matching the component (B). Finally, the close to upright NO

molecules give rise to the lowest four frequencies including the symmetric coupling mode at 1698 cm^{-1} corresponding to the (C) component. Regarding the other contribution calculated at 1614 cm^{-1} (**Table 3**), it seems however that the agreement with experimental data is less satisfactory for this configuration which could be an indication that the parallel configuration is more relevant for the experimental data. Coming back to the second derivative analysis (**Figure 2 b**), we have proposed that the overlap between NO-CoMoS and NO-Co_9S_8 in region (A) is limited to the highest frequency at ca. 1859 cm^{-1} (A). For CoMoS/δθ-Al_2O_3, the intense shoulder at 1846 cm^{-1} may thus correspond to the NO adsorption on the specific Co sites present in the CoMoS phase (and not in Co_9S_8) as identified by DFT calculations. Since component (A') is not experimentally observed neither on the non-promoted MoS_2 (even at high NO coverage) and nor on the Co_9S_8 phase but is present on the promoted MoS_2/δθ-Al_2O_3 samples, it must be considered as the signature of the presence of the promoter either at the M-edge or eventually at the S-edge with NO in upright-tilted configuration, in CoMoS/δθ-Al_2O_3 (considering the aforementioned restrictions). The incidence of this key feature will be further analyzed in the next section devoted to support effects.

3.3 Comparison with γ–Al_2O_3 and SiO_2 supported samples

To evaluate the sensitivity of the NO probe IR spectroscopy and identify potential support effect on the sulfided phase, the second derivatives method was applied to spectra of NO adsorbed on CoMoS supported on γ-Al_2O_3, δθ-Al_2O_3 and SiO_2 (**Figure 3**).

Analyzing firstly the three IR spectra (**Figure 3 a**), it appears that the two alumina supported catalysts exhibit rather similar features, whereas the spectrum of NO-CoMoS/SiO_2 reveals obviously several features which differ from the alumina supported catalysts. The three main components at (A), (B) (C) are slightly shifted at higher frequencies and have narrower full width at half maximum (FWHM) than the alumina supported catalysts. This observation might result from several effects. First, we cannot exclude

an indirect effect of the silica support on the NO vibration. Due to the different Brønsted acidity of the hydroxyl groups and different electrostatic fields exerted by alumina and silica,[58] the NO interaction with the sulfided phase is indirectly perturbed by the support which slightly shifts the NO frequency on aluminas with respect to silica. Moreover, the narrower FWHM of components (A) and (B) may indicate that the speciation of sites involved in NO adsorption are less numerous.

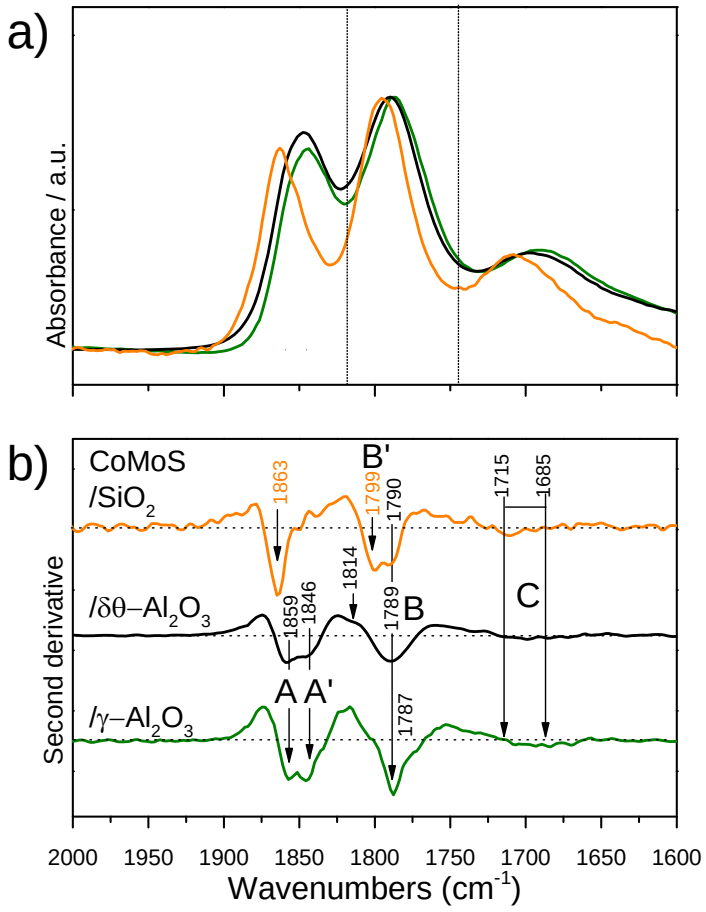

Figure 3. (a) IR spectra of sulfided CoMoS supported on γ-Al_2O_3 (green), δθ-Al_2O_3 (black) and SiO_2 (orange) (normalized per gram of catalyst) after 5 min contact in NO (P = 70 mbar) and subsequent evacuation at 298K; and (b) corresponding second derivative spectra (similar code color). Note: on silica, spectrum reports low signal to noise ratio.

511 Considering now the second derivative analysis, the four previously discussed components (A), (A'), (B)
512 and (C) are actually observed for both alumina supported CoMoS catalysts. In this case, the components
513 at high wavenumbers correspond to two minima (A) at 1859 cm^{-1} and (A') at 1846 cm^{-1}, whereas the
514 silica supported catalyst exhibits only one minimum (A) at 1863 cm^{-1} (with a very small shoulder at 1849
515 cm^{-1}). As previously analyzed, since IR spectrum of NO-Co_9S_8/δθ-Al_2O_3 reveals a highest band (A) very
516 close to 1859 cm^{-1}, the second peak at 1846 cm^{-1} (A') is unambiguously assigned to NO on the CoMoS
517 sites on the alumina supported catalysts. At high NO coverage, (A') contribution should correspond to
518 multi-nitrosyl complexes stabilized on specific cobalt sites located either on the M-edge or on the S-edge
519 (with NO in upright-tilted configuration) of the CoMoS phase according to DFT calculations (**Table 3**).
520 Hence, the relative intensities of (A) and (A') components in the second derivatives differ from one
521 support to another and may consequently be the signature of the promotion degree reached in the CoMoS
522 phase: in particular, the intensity of (A') component decreases significantly on silica which indicates that
523 the Co-promoted sites are strongly diminished on silica. The comparison of the relative intensity of the
524 (A') and (A) components on the two alumina supports indicate (as expected) that the cobalt sites present
525 in the mixed CoMoS phase are similar than the ones present on silica. Nevertheless, we can notice that
526 the relative intensities of (A) and (A') differ slightly, which may also be a signature of the impact of the
527 alumina polymorphs on the CoMoS active phase.
528 Coming back to silica, the main contribution (B) is actually composed of two distinct contributions at
529 1799 cm^{-1} (B') and 1790 cm^{-1} (B) which is not the case for the Al_2O_3 supported samples. Two
530 complementary interpretations can be furnished. First of all, coming back to our previous DFT
531 calculations at maximal NO coverage (**Table 3**), the calculated frequencies of NO adsorbed on the cobalt
532 promoted M-edge and S-edge (1774 and 1782/1787 cm^{-1} respectively), and on the non-promoted M-edge
533 (1809 cm^{-1}). Thus, the promoted M-edge and S-edge may correspond to the contribution (B), while the
534 band (B') may originate from the non-promoted M-edge. Since on the silica supported sample, the level

535 of cobalt promotion is expected to be low compared to alumina supported catalysts (due to the low
536 intensity of (A')), the two components (B) and (B') should preferentially correspond respectively to the
537 non-promoted M-edge and to the promoted S-edge. If so, the respective behaviors of (A') and (B') are
538 decoupled on silica : the (A') component diminishes while (B') remains. Hence, (A') should be assigned
539 predominantly to the Co-promoted M-edge site, whereas (B') to the Co-promoted S-edge site. The second
540 possible interpretation is that the slightly shifted (B) component can also be assigned to the NO adsorbed
541 on Co_9S_8 phase (as the (A) component is also shifted), while the (B') still corresponds mainly to non-
542 promoted sites and/or some promoted S-edge sites.
543 Regarding the third main contribution (C), different maxima (with some shifts) are identified which may
544 also be assigned to the presence of non-promoted MoS_2 and promoted sites as calculated by DFT. If we
545 consider the reference sample NO-Co_9S_8/δθ-Al_2O_3, it appears that the positions of bands (A) and (B) are
546 rather close to the ones of NO-CoMoS/SiO_2.

547 3.4 Chemometric analysis

548 A chemometric approach was applied to the spectra series of NO sorbed (in excess) on CoMoS phase
549 supported on alumina and silica. The objective is to attempt to further identify the spectral features of
550 each population of surface sites on the sulfided phase probed by NO as a function of contact time in order
551 to distinguish the contribution of various site populations according to their intrinsic affinity for NO.
552 Chemometric approach undertaken on the non-promoted MoS_2/δθ-Al_2O_3 (**Figure 4)** shows that two main
553 reference spectra (RS) are needed to explain more than 99% of the variance IR spectra evolution recorded
554 as function of NO contact time (**Table S4.1**).

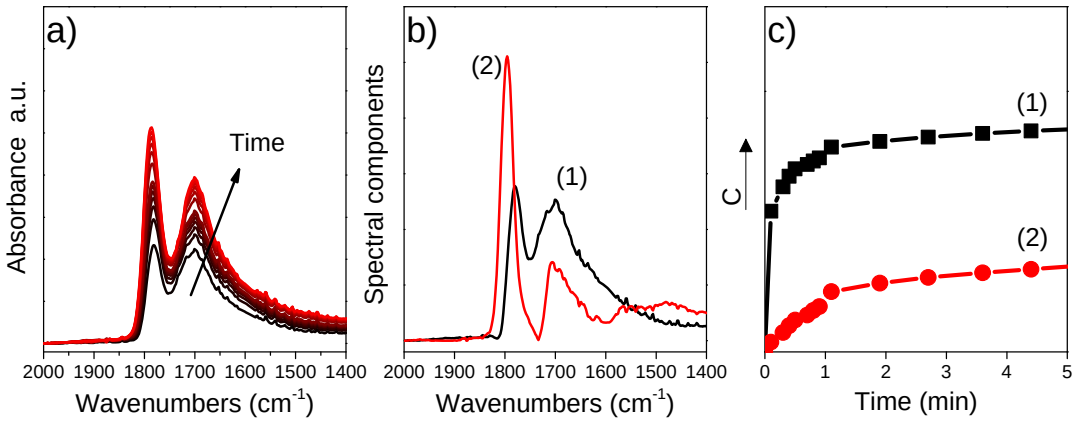

Figure 4. (a) Evolution in the IR spectra (background subtracted) of $MoS_2/\delta\theta$-Al_2O_3 as a function of NO contact time at RT (from black to red); (b) Corresponding MCR decomposition into 2 reference spectra RS(1) and RS(2); (c) profiles of proportion of each reference spectrum: C is dimensionless and expressed as the relative contribution of the three reference spectra in (b) to the spectra displayed in (a). The reference spectra are normalized as function of the total IR absorbance area in the 2000 – 1400 cm^{-1}.

First, the concentration profile of RS(1) increases as soon as NO is introduced in the IR cell (t = 0). Once the concentration of RS(1) reaches a plateau, then concentration of RS(2) starts to increase, which may indicate that populations of RS(1) and RS(2) are linked. Contributions of RS(2) are found at higher wavenumbers than those of RS(1). This trend can be interpreted in two ways. RS(2) could be related to the same population of surface sites as RS(1) but since it appears at higher NO coverage it would correspond to a mononitrosyl to dinitrosyl transition. However, the mononitrosyl to dinitrosyl transition would imply that RS(1) should completely progressively disappear at the expense of RS(2). Since it is obviously not the case in **Figure 4 c)**, this suggests that two distinct types of sites populations are revealed by the chemometric analysis. These two families of sites could be located on the M-edge and S-edge respectively. DFT calculations have shown that the (B) and (C) components of NO adsorbed on the S-edge are also shifted to higher frequency values than on the M-edge **(Table S4.1)**. If so, this implies that the chemometry analysis is able to reveal the presence of the two edges exposed on the MoS_2 nano-crystallites as proposed in previous experimental[7] and theoretical[9] analysis.

Considering now CoMoS/δθ-Al_2O_3, three main reference spectra RS (1-3) are necessary to explain the IR spectra evolution (**Table S4.2**). The profiles of the proportion of the different RS increase as soon as NO is introduced in the IR cell, which may indicate that the RS are not dealing with the same populations of surface sites interacting with NO. **Figures 5 b) and c)** illustrates how the chemometric analysis enables to distinguish the CoMoS phase from the MoS_2 (**Figure 4**) and Co_9S_8 phases (**Figure S4.1**).

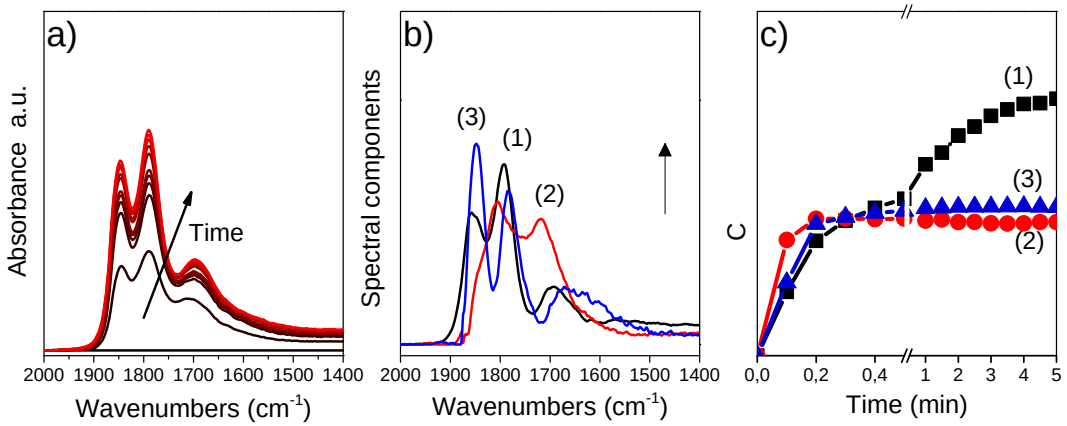

Figure 5. (a) Evolution in the IR spectra (background subtracted) of CoMoS/δθ-Al_2O_3 as a function of NO contact time at RT (from black to red); (b) Corresponding MCR decomposition into 3 reference spectra and (1–3); (c) Profiles of the proportion of each reference spectrum: C is dimensionless and expressed as the relative contribution (area) of the three reference spectra in (b) to the spectra displayed in (a). Time axis of c) panel is broken in order to visualize the evolution in the very first minute of NO contact.

The reference spectra (1) and (3) report 3 main contributions located at 1857-1847 and 1792-1785 and 1695-1670 cm^{-1} referred as A-A', B, C in **Table S4.2**. The shape of the profiles indicates that different surface sites are contributing in these three reference spectra. DFT calculations have demonstrated that the partially promoted M-edge and fully promoted S-edge sites interacting with NO at high coverage may explain the (A')-(B) and (B)-(C) components respectively. Since the concentration profiles of the different RS increase as soon as NO is introduced in the IR cell, this also confirms that the (A')-(B) and (B)-(C) components are not linked together and do correspond to two populations of sites which could be

595 the promoted M-edge and/or S-edge as shown by DFT calculations. Consequently, RS(3) could
596 correspond to the spectral feature of NO on the promoted CoMoS phase. Considering RS(1), the
597 contribution centered at high wavenumbers 1857 cm^{-1} (A) is close to what is observed for the supported
598 Co_9S_8 reference material (**Figure 2**). It seems that RS(1) corresponds to a mix between Co_9S_8 and MoS_2
599 based phases since component (C) is also present in the spectrum (**Figure 5 b**). The reference spectrum
600 RS(2) reports two maxima at 1805 and 1718 cm^{-1} for components (B) and (C) respectively. In that case,
601 the nature of the corresponding sulfided phase population is expected to be non-promoted. Interestingly,
602 **Figure 5 c** shows that this population of sites is the first one to be revealed at small NO contact time. This
603 could correspond to the stronger adsorption energy of Mo sites with respect to Co sites as determined by
604 DFT calculations. Moreover, it is also interesting to stress that the component (C) at 1714 cm^{-1} seems to
605 be specific of the non-promoted phase whereas the cobalt sulfided phases reveal contributions to
606 component (C) at lower wavelengths (1695 and 1670 cm^{-1}) which is consistent with the previous DFT
607 and IR analysis. The intensity of component (C) is also enhanced on RS(2).
608 Hence, from the chemometric analysis, it becomes possible to distinguish different populations of phases
609 present on $\delta\theta$-Al_2O_3 support which report different behavior in presence of NO: RS(1) assigned to a
610 combination of Co_8S_9 and MoS_2 (promoted/non-promoted); RS(2) due to MoS_2 phase and RS(3) due to a
611 mixture of promoted and non-promoted MoS_2 phases.
612 In order to explore also with this chemometric technique, the effect of the support, similar decompositions
613 have been undertaken for silica and γ-Al_2O_3 supported CoMoS catalysts. For sake of clarity, the detailed
614 analysis of these spectra are reported in **Supplementary information 4**. To summarize them, it appears
615 that the chemometric analysis is able to reveal different spectroscopic features for these two supported
616 catalysts from the $\delta\theta$-Al_2O_3 supported ones. In particular, two (respectively one) reference spectra were
617 required to explain the evolution of the IR spectrum on silica (respectively on γ-Al_2O_3). It appears thus
618 more difficult to totally decouple the evolution of the three families of sites observed on $\delta\theta$-Al_2O_3 in the

619 case of silica and γ-Al_2O_3 supported catalyst. This smaller number of reference spectra can also be
620 interpreted as the signature of the presence of less numerous surface site species. In particular, even if the
621 presence of Co_9S_8 phase cannot be discarded on γ–Al_2O_3 supported sample, its concentration is probably
622 not high enough to be recovered by the chemometric analysis as it is the case on δθ–Al_2O_3 and SiO_2
623 supports. On silica, a weaker concentration of promoted CoMoS sites at the profit of the Co_9S_8 phase and
624 non-promoted MoS_2 phase can be at the origin of the two reference spectra identified by chemometry.
625
626 3.5 Impact for hydrodesulfurization (HDS) catalysis
627 According to previous experimental studies,[1, 59, 60] it is now well-established that the formation of the
628 mixed CoMoS phase is a key parameter for reaching high HDS catalytic activity. Thus, featuring by IR
629 spectroscopy the degree of the promotion and the nature of cobalt sites present at the edges of the CoMoS
630 nano-crystallites is critical. According to previous DFT calculations,[10, 11] cobalt atoms located at the
631 M-edge are less stable than the ones located at the S-edge. Thus, the decrease of the (A') component
632 could be principally driven by a lower concentration of cobalt atoms located on the M-edge in particular.
633 It seems also to be simultaneously accompanied by an increase of the (C) component in the region of
634 1700-1714 cm^{-1} assigned to mononitrosyl or dinitrosyl on the non-promoted M-edge (**Figure 2**). As a
635 consequence, the IR spectroscopic analysis (**Figure 3**) suggests that part of this silica supported sample
636 may contain a larger proportion of the Co_9S_8 phase at the expense of the cobalt promoted MoS_2 phases.
637 This lower concentration of the mixed CoMoS sites on silica is thus at the origin of the lower HDS
638 activities (normalized per Mo atom) generally reported for silica supported catalysts compared to the
639 alumina supported ones (for the same Co/Mo ratio and Mo loading).[31-34, 38] Moreover, if the decrease
640 of the promotion degree of silica supported CoMoS catalysts corresponds to the loss of cobalt atoms on
641 the M-edge, this would explain the higher selectivity observed in hydrodesulfurization of thiophenic
642 molecules over hydrogenation (HYD) of olefinic compound on silica supported catalysts.[34, 38, 61]

643 Indeed previous experimental and theoretical works[7, 62] show that the HDS/HYD selectivity is
644 correlated to the proportion of cobalt promoted S-edge in the CoMoS active phases. Thus the intrinsic
645 HDS/HYD selectivity of Co promoted S-edge is higher, which would be perfectly coherent with our NO-
646 FTIR analyses revealing that the M-edge would be not promoted on silica support. Regarding the
647 γ– and δθ–alumina polymorphs, the second derivative and chemometric analyses revealed different
648 behaviors which may also help to understand different HDS catalytic activities as a function of the
649 alumina polymorph used as a support.[36] We may in particular suspect that the promotion level of
650 γ–alumina supported CoMoS phase is higher than the one of δθ–alumina supported one. Thus, the
651 different CoMoS sites speciation supported either on silica or on aluminas is well revealed by NO-FTIR
652 spectroscopy, which appears as a useful technique to discriminate between optimal and non-optimal
653 CoMoS active phases featured by the (A') and (C) components.

654 4. CONCLUSIONS

655 By combining FTIR spectroscopy and DFT calculations, we have shown that NO is a relevant molecule
656 to probe and identify the sites of the MoS_2, CoMoS and Co_9S_8 phases on three relevant catalytic supports:
657 δθ-Al_2O_3, γ-Al_2O_3 and SiO_2. To help for the interpretation, we have undertaken periodic boundary DFT
658 calculations of NO adsorbed on the various possible non-promoted MoS_2 and promoted CoMoS sites at
659 various NO and sulfur coverages.

660 Second derivative spectroscopy has been applied to distinguish the overlapping contributions which are
661 not resolved in the initial IR spectrum of alumina and silica supported systems. **Table 4** summarizes the
662 main learning of the present study by combining second derivative analysis, chemometry and DFT
663 calculations regarding NO probe molecule adsorption and site speciation.

Table 4. Summary of site speciation as a function of the different components identified by NO probe molecule according to second derivative analysis, chemometric analysis and DFT calculations undertaken on the various systems of the present study.

Component	ν^a (cm^{-1})	CoMoS		MoS_2		Co_9S_8
		M-edge	S-edge	M-edge	S-edge	
A	1857-1863					✓
A'	1846-1849	✓	✓			
B'	1789-1799				✓	✓
B	1787-1790		✓	✓		
	1714-1716		✓		✓	
C	1697		✓		✓	
	1685-1686		✓	✓	✓	

[a] the wavelength intervals are identified on the various supports: γ-Al_2O_3, $\delta\theta$-Al_2O_3, and SiO_2

The specific contributions (A') at 1846 cm^{-1} and (B) at 1790 cm^{-1} have been identified for alumina supported samples and are assigned to cobalt-promoted sites, while the component (A) at ca. 1859 cm^{-1} is assigned to Co_9S_8. From DFT calculations, it is shown that mononitrosyls on Co site and dinitrosyls on Mo site of the promoted M-edge sites give rise to these (A')-(B) components. Depending on the local configuration (either parallel or upright-tilted) dinitrosyls on the cobalt S-edge give rise to either components (B)-(C) or (A')-(B)-(C) at high NO coverage. In addition, the region (C) is due to dinitrosyls on the promoted S-edge but also to the non-promoted M-edge sites.

The silica supported catalyst revealed a different spectroscopic feature which helped us to refine further the spectroscopic assignment. Indeed, silica supported sample displays a strongly diminished (A') component assigned to the loss of CoMoS sites on the promoted M-edge due to their lower intrinsic stability, previously shown by DFT calculations. However, it exhibits two intense contributions (B') at 1799 cm^{-1} and (B) at 1790 cm^{-1} assigned to the presence of non-promoted M-edge or Co_9S_8, and to promoted S-edge sites, respectively. If the (B) component on silica is assigned to the promoted S-edge, this implies that the (A') is predominantly due to the promoted M-edge.

This spectroscopic approach may thus enable to explain the origin of the lower HDS activities generally reported for silica supported catalysts compared to the alumina ones. More generally, the relative intensity of contributions (A') and (A) should be considered as a good descriptor of the promotion degree of CoMoS on the three supports: γ-Al_2O_3 > $\delta\theta$-Al_2O_3 > SiO_2. As a consequence, NO spectroscopy is a relevant technique to characterize the "intrinsic quality" of the CoMoS phase as a function of the supports: $\delta\theta$-Al_2O_3, γ-Al_2O_3 and SiO_2.

From chemometric analysis of IR spectra series, M-edge and S-edge sites have been identified for MoS_2 supported $\delta\theta$-Al_2O_3 catalyst. Among the different supports investigated, the concentration of promoted sites on the M-edges of the CoMoS phase is the lowest on SiO_2, which is in agreement with the lowest activity and highest selectivity of this support.

The detailed combined spectroscopic and DFT study offers a rational and quantitative description of the nature of edge sites of the MoS_2 and CoMoS phase as a function of the support. This will provide a robust methodology allowing a better control and design of the optimal CoMoS active phase used in hydrotreatment catalysts.

ACKNOWLEDGMENTS

This work was performed using HPC resources from GENCI-IDRIS-CINES (Grant 2017-A0020806134) and the IFPEN supercomputer (ENER110).

REFERENCES

[1] P. Raybaud, H. Toulhoat, Catalysis by Transition Metal Sulfides. From molecular theory to industrial applications., Technip Edition, Paris (France), 2013.

[2] H. Topsøe, B.S. Clausen, F.E. Massoth, Hydrotreating Catalysis - Science and Technology, Springer-Verlag, Berlin/Heidelberg, 1996.

[3] A.D. Gandubert, E. Krebs, C. Legens, D. Costa, D. Guillaume, P. Raybaud, Catal. Today 130 (2008) 149.

[4] S.M.A.M. Bouwens, J.A.R.v. Veen, D.C. Koningsberger, V.H.J.d. Beer, R. Prins, J. Phys. Chem. 95 (1991) 123.

[5] B.S. Clausen, H. Topsøe, R. Candia, J. Villadsen, B. Lengeler, J. Als-Nielsen, F. Christensen, J. Phys. Chem. 85 (1981) 3868.
[6] L.P. Hansen, E. Johnson, M. Brorson, S. Helveg, J. Phys. Chem. C 118 (2014) 22768.
[7] B. Baubet, M. Girleanu, A.-S. Gay, A.-L. Taleb, M. Moreaud, F. Wahl, V. Delattre, E. Devers, A. Hugon, O. Ersen, P. Afanasiev, P. Raybaud, ACS Catal. 6 (2016) 1081.
[8] C. Wivel, R. Candia, B.S. Clausen, S. Mørup, H. Topsøe, J. Catal. 68 (1981) 453.
[9] H. Schweiger, P. Raybaud, G. Kresse, H. Toulhoat, J. Catal. 207 (2002) 76.
[10] E. Krebs, B. Silvi, P. Raybaud, Catal. Today 130 (2008) 160.
[11] H. Schweiger, P. Raybaud, H. Toulhoat, J. Catal. 212 (2002) 33.
[12] M. Saab, P. Raybaud, J. Phys. Chem. C 120 (2016) 10691.
[13] P.G. Moses, B. Hinnemann, H. Topsøe, J.K. Nørskov, J. Catal. 268 (2009) 201.
[14] P. Raybaud, Appl. Catal. A: Gen. 322 (2007) 76.
[15] F. Mauge, J. Lamotte, N.S. Nesterenko, O. Manoilova, A.A. Tsyganenko, Catal. Today 70 (2001) 271.
[16] B. Temel, A.K. Tuxen, J. Kibsgaard, N.Y. Topsoe, B. Hinnemann, K.G. Knudsen, H. Topsoe, J.V. Lauritsen, F. Besenbacher, J. Catal. 271 (2010) 280.
[17] S. Humbert, G. Izzet, P. Raybaud, J. Catal. 333 (2016) 78.
[18] C. Dujardin, M.A. Lélias, J. van Gestel, A. Travert, J.C. Duchet, F. Maugé, Appl. Cat. A: General 322 (2007) 46.
[19] A. Travert, C. Dujardin, F. Maugé, E. Veilly, S. Cristol, J.-F. Paul, E. Payen, J. Phys. Chem. B 110 (2006) 1261.
[20] K.I. Hadjiivanov, Catal. Rev. 42 (2000) 71.
[21] A. Zecchina, M. Rivallan, G. Berlier, C. Lamberti, G. Ricchiardi, Phys. Chem. Chem. Phys. 9 (2007) 3483.
[22] M. Rivallan, G. Ricchiardi, S. Bordiga, A. Zecchina, J. Catal. 264 (2009) 104.
[23] L. Kovarik, N.M. Washton, R. Kukkadapu, A. Devaraj, A.Y. Wang, Y.L. Wang, J. Szanyi, C.H.F. Peden, F. Gao, ACS Catal. 7 (2017) 2458.
[24] N.-Y. Topsøe, H. Topsøe, J. Catal. 84 (1983) 386.
[25] L. van Haandel, E.J.M. Hensen, T. Weber, Catal. Today 292 (2017) 67.
[26] Y. Okamoto, M. Kawano, T. Kawabata, T. Kubota, I. Hiromitsu, J. Phys. Chem. B 109 (2005) 288.
[27] N.-Y. Topsøe, A. Tuxen, B. Hinnemann, J.V. Lauritsen, K.G. Knudsen, F. Besenbacher, H. Topsøe, J. Catal. 279 (2011) 337.
[28] N.-Y. Topsøe, H. Topsøe, J. Catal. 75 (1982) 354.
[29] A. Travert, C. Dujardin, F. Maugé, E. Veilly, S. Cristol, J.-F. Paul, E. Payen, J. Phys. Chem. B 110 (2006) 1261.
[30] P. Euzen, P. Raybaud, X. Krokidis, H. Toulhoat, J.L. Le Loarer, J.P. Jolivet, C. Froidefond, Alumina, in: Handbook of Porous Solids, Wiley-VCH Verlag GmbH, 2008, pp. 1591.

744 [31] C. Roukoss, D. Laurenti, E. Devers, K. Marchand, L. Massin, M. Vrinat, C. R. Chim. 12 (2009) 683.
745 [32] T.K.T. Ninh, D. Laurenti, E. Leclerc, M. Vrinat, Appl. Catal. A: Gen. 487 (2014) 210.
746 [33] L. Kaluza, D. Gulkova, Z. Vit, M. Zdrazil, Appl. Catal. A: Gen. 324 (2007) 30.
747 [34] Y. Okamoto, K. Ochiai, M. Kawano, K. Kobayashi, T. Kubota, Appl. Catal. A: Gen. 226 (2002) 115.
748 [35] J. Ramirez, S. Fuentes, G. Diaz, M. Vrinat, M. Breysse, M. Lacroix, Appl. Catal. 52 (1989) 211.
749 [36] D. Laurenti, P.N. Bo, C. Roukoss, E. Devers, K. Marchand, L. Massin, L. Lemaitre, C. Legens, A.A.
750 Quoineaud, M. Vrinat, J. Catal. 297 (2013) 165.
751 [37] S. Brunet, D. Mey, G. Perot, C. Bouchy, F. Diehl, Appl. Catal. A: General 278 (2005) 143.
752 [38] G. Muralhidar, F.E. Massoth, J. Shabtai, J. Catal. 85 (1984) 44.
753 [39] D. Costa, C. Arrouvel, M. Breysse, H. Toulhoat, P. Raybaud, J. Catal. 246 (2007) 325.
754 [40] J. Jaumot, R. Gargallo, A. de Juan, R. Tauler, Chemom. Intell. Lab. Syst. 76 (2005) 101.
755 [41] M. Rivallan, E. Seguin, S. Thomas, M. Lepage, N. Takagi, H. Hirata, F. Thibault-Starzyk, Angewandte
756 Chemie International Edition 49 (2010) 785.
757 [42] G. Kresse, J. Furthmüller, Phys. Rev. B 54 (1996) 11169.
758 [43] G. Kresse, J. Joubert, Phys. Rev. B 59 (1999).
759 [44] G. Kresse, J. Hafner, Phys. Rev. B 47 (1993) 558.
760 [45] J.P. Perdew, Y. Wang, Phys. Rev. B 45 (1992) 13244.
761 [46] J.P. Perdew, J.A. Chevary, S.H. Vosko, K.A. Jackson, M.R. Pederson, D.J. Singh, C. Fiolhais, Phys. Rev. B
762 46 (1992) 6671.
763 [47] J.P. Thielemann, J. Kröhnert, C. Hess, J. Phys. Chem. C 114 (2010) 17092.
764 [48] Z. Shuxian, W.K. Hall, G. Ertl, H. Knozinger, J. Catal. 100 (1986) 167.
765 [49] A. Kazusaka, R.F. Howe, J. Catal. 63 (1980) 447.
766 [50] J.E. Herrera, L. Balzano, A. Borgna, W.E. Alvarez, D.E. Resasco, J. Catal. 204 (2001) 129.
767 [51] S. Kasahara, T. Shimizu, M. Yamada, Catal. Today 35 (1997) 59.
768 [52] N. Koizumi, K. Takahashi, M. Yamazaki, M. Yamada, Catal. Today 45 (1998) 313.
769 [53] L. Portela, P. Grange, B. Delmon, Catal. Rev. 37 (1995) 699.
770 [54] P. Raybaud, J. Hafner, G. Kresse, S. Kasztelan, H. Toulhoat, J. Catal. 189 (2000) 129.
771 [55] P. Raybaud, J. Hafner, G. Kresse, S. Kasztelan, H. Toulhoat, J. Catal. 190 (2000) 128.
772 [56] X.-D. Wen, T. Zeng, Y.-W. Li, J. Wang, H. Jiao, J. Phys. Chem. B 109 (2005) 18491.
773 [57] C. Lamberti, A. Zecchina, E. Groppo, S. Bordiga, Chem. Soc. Rev. 39 (2010) 4951.
774 [58] F. Leydier, C. Chizallet, D. Costa, P. Raybaud, Chem. Commun. (Cambridge, U. K.) 48 (2012) 4076.
775 [59] A. Gandubert, E. Krebs, C. Legens, D. Costa, D. Guillaume, P. Raybaud, Catal. Today 130 (2008) 149.
776 [60] C. Wivel, R. Candia, B.S. Clausen, S. Mørup, H. Topsøe, J. Catal. 68 (1981) 453.
777 [61] M.F. Li, H.F. Li, F. Jiang, Y. Chu, H. Nie, Catal. Today 149 (2010) 35.
778 [62] E. Krebs, B. Silvi, A. Daudin, P. Raybaud, J. Catal. 260 (2008) 276.